Article

1D Perovskitoid as Absorbing Material for Stable Solar Cells

Fan Xu [1,2], Yujing Li [1], Na Liu [1], Ying Han [1], Meishuai Zou [1,*] and Tinglu Song [1,*]

1   Experimental Center of Advanced Materials, School of Materials Science and Engineering,
    Beijing Institute of Technology, Beijing 100081, China; xuf21@mcmaster.ca (F.X.); yjli@bit.edu.cn (Y.L.);
    3120170530@bit.edu.cn (N.L.); 3120195664@bit.edu.cn (Y.H.)
2   Department of Materials Science and Engineering, McMaster University, 1280 Main ST W,
    Hamilton, ON L8S 4L8, Canada
*   Correspondence: zoums@bit.edu.cn (M.Z.); song@bit.edu.cn (T.S.)

Abstract: The instabilities of perovskite solar cells hinder their commercialisation. To resolve this problem, a one-dimensional (1D) perovskitoid, $PyPbI_3$, was fabricated, and its structure and photovoltaic performance were investigated in this work. XPS and FTIR results suggest hydrogen bonds existed in the 1D hexagonal $PyPbI_3$. Stability measurements indicate that 1D perovskitoid is much more stable than the commonly employed FA-based perovskite. In addition, solar cells adopting $PyPbI_3$ as an absorbing layer led to a device lifetime of one month. Our results suggest that 1D perovskitoid has great potential to be employed in solar cells.

Keywords: perovskite solar cell; 1D perovskitoid; stability; photovoltaic material; hydrogen bonds

1. Introduction

The growing demand for renewable energy in the 21st century has made photovoltaics (PV) a popular research area [1,2]. Among all PV cells, perovskite solar cells (PSC) have attracted lots of interest. The power conversion efficiency of PSC has achieved a maximum of 25.5% within only one decade since its original report in 2009 [3]. The rapid development of PSC can be attributed to its long diffusion length [4], high absorption coefficient [5], tunable bandgap [6] and so forth.

However, the commonly employed perovskite is not stable when exposed to moisture or thermal stress [7,8], which leads to a short lifetime of the fabricated solar cell devices, thereby limiting their commercialisation. Various attempts have been made to overcome these instability problems, such as interface engineering [9–11], strain engineering [12,13], encapsulation [14,15], etc., yet the PSC lifetime is still far from satisfactory; i.e., most PSCs would lose most of their initial efficiency within only hundreds of hours under ambient conditions. In this regard, replacing the hydrophilic methylammonium (MA) and formamidinium (FA) cations seems imperative and inevitable.

Most recently, the employment of carbocyclic cations with strong hydrophobic nature to form a perovskite structure has attracted lots of interest. For instance, Pering et al. (2017) [16] employed four-membered carbocyclic ring azetidine as cation to form perovskite ($AztPbI_3$). Despite the enhanced moisture resistance, the $AztPbI_3$ is found to be thermodynamically unstable and exhibits low crystallinity [16]. To resolve this, Zheng et al. (2018) [17] proposed a new perovskite material, aziridinium lead iodide ($AzrPbI_3$), which possesses three-membered carbocyclic rings. According to the authors' simulation results, the $AzrPbI_3$ exhibits good thermodynamic stability as well as a low bandgap of 1.49 eV, which is comparable to that of $MAPbI_3$ [18]. However, fabricating such materials seems impractical, as aziridine molecules are highly toxic [19]. In addition, recent reports on low-dimensional Bi and Sb-based halide semiconductors have also attracted lots of interest [20–25], due presumably to their good environmental stability as an absorber layer in solar cells.

Based on previous attempts, a five-membered ring-based pyrrolidinium lead iodide (PyPbI$_3$) was first introduced by our group in 2019 [26], which exhibited a 1D "perovskitoid" structure [27], and immediately attracted lots of interest [28–33]. Although promising results have been achieved in solar cell applications employing PyPbI$_3$ as interfacial modification agents to either improve device stability and efficiency [28,30,31] or to control the crystallization process of the 3D MA-based perovskite [32], the application of PyPbI$_3$ as a single absorbing layer has not been reported so far. Therefore, it will be of great significance to explore the potential of such perovskitoid as absorbing material for solar cell applications. Moreover, the structure of PyPbI$_3$ film remains ambiguous [32], which hinders its practical applications.

It is, therefore, the purpose of the current report to evaluate the feasibility of 1D perovskitoids, such as PyPbI$_3$, as a single absorbing layer in PSCs, as well as to investigate its structural properties. Based on the results of XRD, X-ray photoelectron spectroscopy (XPS) and FTIR, we were able to confirm the hexagonal structure of PyPbI$_3$, as well as the interatomic force between Py cation and PbI$_2$ lattice. The stability of 1D perovskitoid film is much more stable than commonly employed FA-based perovskite, as revealed by stability measurements. Lastly, we employed PyPbI$_3$ as absorbing material to fabricate solar cells, yielding a device lifetime of more than one month. In addition, the outlook of 1D perovskitoid in photovoltaics is briefly discussed in the summary part.

2. Materials and Methods

2.1. Materials

Pyrrolidinium hydroiodide (98%, TCI America, Portland, Oregon, USA), PbI$_2$ (99.999%, Sigma-Aldrich, St. Louis, MO, USA), isopropanol (IPA, 99.99%, Sigma-Aldrich, St. Louis, MO, USA), N,N-dimethylformamide (DMF, 99.99%, Sigma-Aldrich, St. Louis, MO, USA), Dimethyl sulfoxide (DMSO, 99.9%, Sigma-Aldrich, St. Louis, MO, USA), Spiro-OMeTAD (Xi'an Polymer Light Technology Corp., Xi'an, Shaanxi, China), bis(trifluoromethane)sulfonimide lithium salt (99.95%, Aldrich, St. Louis, MO, USA), 4-tertbutylpyridine (99.9%, Sigma-Aldrich, St. Louis, MO, USA) and ITO substrates.

2.2. Device Fabrication

To fabricate perovskite solar cell devices, the ITO substrate was first washed with distilled water and ethanol, two times each. After 20 min of UV–O$_3$ treatments, the SnO$_2$ electron transport layers (ETLs) were spin-coated on ITO substrates from the SnO$_2$ colloidal solutions and annealed on a hot plate at the displayed temperature of 150 °C for 30 min in ambient air. For the PyPbI$_3$ layer, sequential deposition method was adopted. Thirty microlitres of lead iodide solutions were first spin-coated at 2300 rpm for 30 s and annealed at 70 °C for 1 min. Then, 80 µL of PyI solutions were spin-coated at 2000 rpm for 30 s. The as-fabricated films were then annealed at 150 °C for 30 min in air. Next, 30 µL Spiro-OMeTAD solution doped with LiTFSI and tBP was deposited at 3000 rpm for 30 s. Finally, 100 nm Ag was thermally evaporated as a counter electrode under a pressure of 5×10^{-5} Pa on top of the hole transport layer to form the metal contact.

2.3. Characterizations

The absorption spectra were recorded by Hitachi UH4150 spectrophotometer. X-ray diffraction (XRD) patterns were obtained using a Rigaku D/Max 2200 with Cu Kα as the X-ray source. X-ray photoelectron spectroscopy (XPS) measurement was carried out on PHI Quantera-II SXM. The FTIR spectra were measured by a Nicolet 6700 FT-IR spectrometer. The current density–voltage characteristics of photovoltaic devices were obtained using a Keithley 2400 source-measure system. The photocurrent was measured under AM 1.5 G illumination at 100 mW/cm^2 using a Newport Thermal Oriel 91192 1000 W solar simulator. The light intensity was calibrated using a KG-5 Si diode. The thin film morphology was measured using a scanning electron microscope (SEM) (S4800).

The calculated XRD data were obtained from our previous report [26]. In short details, the calculations were performed using SHELXTL crystallographic software package. Symmetry analysis of the model using PLATON revealed that no obvious space group change was needed. In the refinement, the commands EDAP and EXYZ were used to restrain some of the related bond lengths and bond angles.

3. Results

3.1. Fabrication and Characterizations of 1D Perovskitoid Films

The PyPbI$_3$ films were fabricated via a simple sequential deposition method [34], as schematically illustrated in Figure 1. The details are shown in the experimental section. Previous reports suggest that PyPbI$_3$ may exhibit two different crystal structures, such as hexagonal [26] and orthorhombic [32] phases. However, during our fabrication, all obtained PyPbI$_3$ were crystallized following the same hexagonal space group P6$_3$/mmc, which was confirmed by powder XRD measurements. As shown in Figure 2a, the diffraction peaks of the experimental PyPbI$_3$ film correspond well with its single-crystal XRD data, suggesting the formation of hexagonal PyPbI$_3$ in the film. In general, 1D perovskitoid may exhibit diffraction peaks below 10° [35]. However, all peaks of 1D PyPbI$_3$ are above 10°, with the lowest peak located at around 11° (Figure 2a), which is consistent with other perovskitoid [27]. This might be attributed to their various lattice parameters.
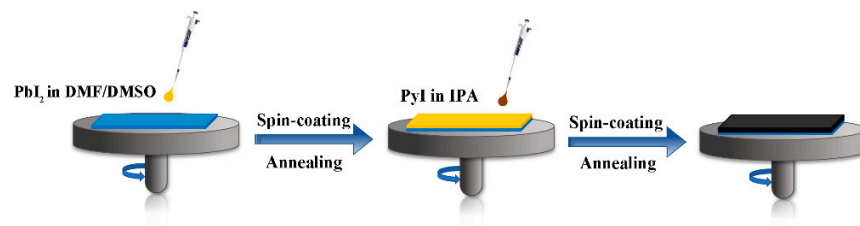

Figure 1. Schematic illustration of the fabrication of PyPbI$_3$ film.
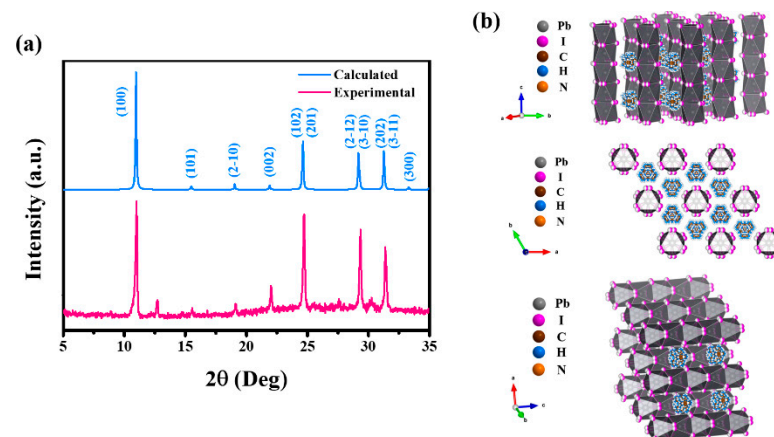

Figure 2. (**a**) XRD results of the calculated and experimental PyPbI$_3$ film. (**b**) Crystal structure of PyPbI$_3$ single crystal. More structure details of PyPbI$_3$ were summarized and discussed in our previous work [26]. Adapted from Ref [26] with permission from The Royal Society of Chemistry.

The microscopic crystal structures of PyPbI$_3$ viewed from different directions are illustrated in Figure 2b; as can be observed, lead iodide octahedrons were arranged in a face sharing method, with Py$^+$ cations located in between them, indicating the 1D characteristics of PyPbI$_3$ [36]. However, the positions and interactions between pyrrolidinium rings and lead iodide lattice remain unresolved (a large cluster of atoms lies in between each chain, Figure 2b), as it is not easy to precisely detect low mass elements such as carbon, nitrogen and hydrogen with XRD measurements. This may result in uncertainty in determining the

exact role of Py$^+$ cations; i.e., the C and N atoms may have interactions with iodides, or they may only maintain the charge balance in crystal lattices [37,38].

X-ray photoelectron spectroscopy (XPS) has been widely employed as a powerful tool to evaluate the interactive forces between atoms in the molecule [39]. Therefore, to further understand the role of organic cations, we conducted XPS measurements to PyI and PyPbI$_3$ crystals, respectively. The results were illustrated in Figure 3a–c. The total XPS spectrum is shown in Figure 3a. Compared to PyI, an extra binding peak for Pb element was found in PyPbI$_3$, indicating the reaction between PyI molecules and PbI$_2$ chains. In addition, the N1s and I3d spectrums exhibit an energy blue shift of more than 3 eV, suggesting a higher binding energy in 1D PyPbI$_3$ than that in PyI powder. This indicates that there is a strong interaction force between Py$^+$ cations and [PbI$_3$]$^-$ octahedra cages, i.e., the hydrogen bonding between N-H and I, bonding them together [37,38]. The existence of hydrogen bonds was further confirmed by FTIR [40] (Figure 3d). The interaction forces between the Py cations and inorganic chains may help to keep the perovskitoid phase unchanged when exposed to external stress such as moisture, since more energy is required to break the hydrogen bonds [38]. The enhanced stability of PyPbI$_3$ observed in the next section could thus be attributed to not only the hydrophobic nature [19] of Py molecule but also their hydrogen bonds.
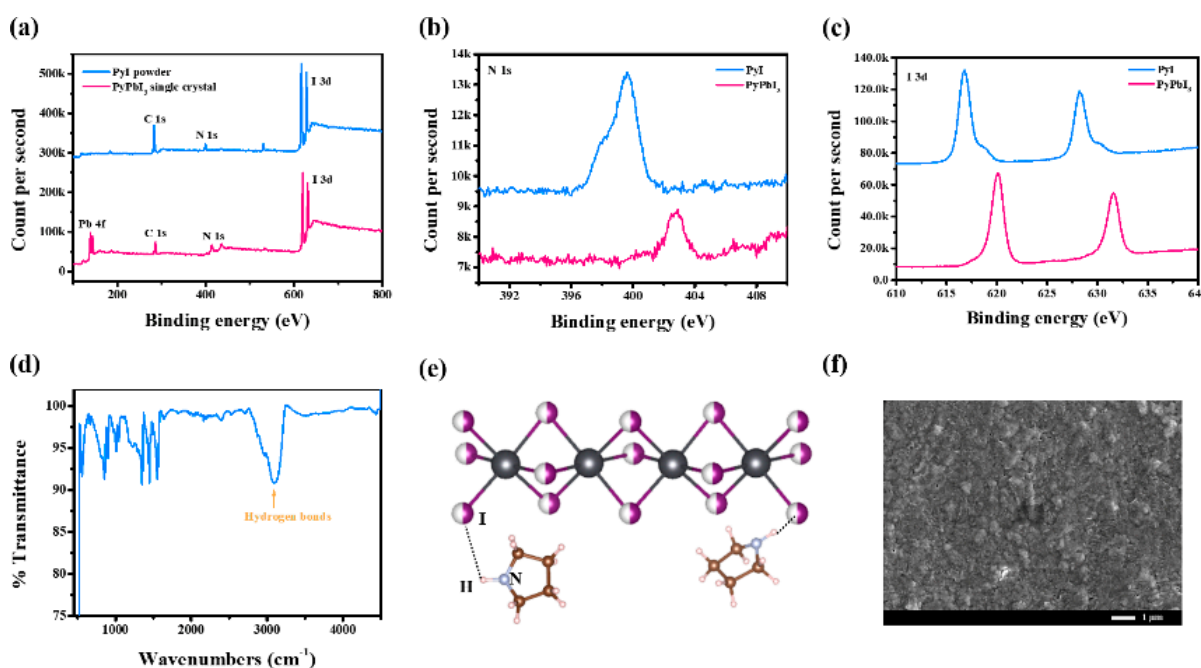

Figure 3. XPS results of the (**a**) whole spectrum, (**b**) N1s and (**c**) I3d of PyI and PyPbI$_3$ crystals. (**d**) FTIR spectra of PyPbI$_3$. Reproduced from Ref [29] with permission from The Royal Society of Chemis-try. (**e**) Schematic illustration of hydrogen bonds in PyPbI$_3$. (**f**) Planar SEM image of PyPbI$_3$ film.

Moreover, the surface morphology of the film was evaluated via SEM technique, which exhibited many small grains (Figure 3f), indicating the formation of 1D perovskitoid [27].

3.2. Stability Measurements of 1D Perovskitoid Films

Next, we investigated the stability of PyPbI$_3$ perovskite films. To make a comparison, two different perovskites, PyPbI$_3$ and FA-based perovskite, were both prepared and evaluated via XRD and UV absorption spectra. All prepared films were stored under ambient conditions with a relative humidity (RH) of 50 ± 5%. The XRD results of PyPbI$_3$ before and after one week are shown in Figure 4a, which show the same patterns, indicating the good environmental stability of PyPbI$_3$. In contrast, the FA-based perovskite film degraded into photoinactive δ-phase after 1 week in air, as is demonstrated in Figure 4b.
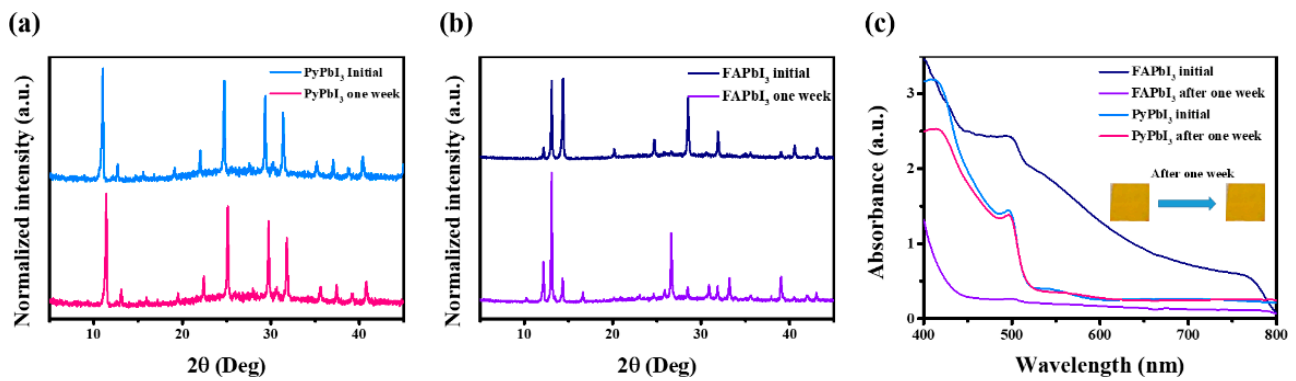
Figure 4. (**a**) XRD patterns of PyPbI$_3$ (**b**) and FAPbI$_3$, and (**c**) UV absorption results of PyPbI$_3$ and FA-based perovskite before and after one week in ambient condition; inset shows the photograph of PyPbI$_3$ perovskite film before and after one week.

Figure 4c illustrates the UV absorption spectra for these films. As can be observed, the FAPbI$_3$ film exhibited a drastic decrease in light absorbance over the whole visible range after 7 days. In contrast, the absorption onset of PyPbI$_3$ film exhibited no obvious change after one week. The photographs of PyPbI$_3$ film before and after one week were presented in the inset of Figure 4c. The color of the film remained unchanged, which is consistent with the XRD and UV results. The above results indicate that PyPbI$_3$ is much stable than FAPbI$_3$.

3.3. Photovoltaic Performance of 1D Perovskitoid Solar Cells

To evaluate the photovoltaic performance of PyPbI$_3$ solar cells, we fabricated PSCs employing ITO/SnO$_2$/PyPbI$_3$/Spiro-OMeTAD/Ag configuration. The J–V curve of the best device is shown in Figure 5a. The photovoltaic parameters were also summarized in the figure, with V$_{oc}$ of 0.74 V, J$_{sc}$ of 0.94 mA/cm^2, FF of 28.05, PCE of 0.3%. The series and shunt resistance of the device were measured to be 6245 and 9483 Ω, respectively, via a Keithley 2400 source-measure system. Based on the literature [16] and absorption results (Figure 4c), the onset of PyPbI$_3$ light absorption was inferred to be around 520 nm. The non-absorption loss may significantly reduce the device photocurrent. While the V$_{oc}$ is comparable to that of AzPbI$_3$ [16] and CsPbI$_3$ [41], the J$_{sc}$ is as low as 1.0 mA/cm^2. The low J$_{sc}$ might be attributed to the relatively large bandgap of PyPbI$_3$, resulting in its low FF and PCE [31,42]. Apart from the bandgap, we also investigated interfacial properties between perovskitoid and CTLs by presenting the energy band diagram of PyPbI$_3$ solar cell [31,39]. As demonstrated in Figure 5b, such energy alignment prevents the back diffusion of electrons and holes toward HTL and ETL, respectively, which is favorable for PV applications. However, the relatively large energy offset (1.31 eV and 0.49 eV for electrons and holes, respectively) may also induce severe voltage and current loss [43], thereby deteriorating device performance. Future work on device modification may be focused on these two aspects. It should be noted that the dark J–V curves can also reveal important cell parameters such as leakage current [44,45]. We expect future investigation on device physics employing this powerful method to gain more insights.

The device stability of PyPbI$_3$ PSCs was also evaluated. Ten solar cell devices were prepared and measured for reliability analysis. All devices were stored in ambient conditions with RH of 65 $\pm$ 5% and temperature of 22 $\pm$ 3 °C. As illustrated in Figure 5c, even after one month in air, the PCE of PyPbI$_3$ PSCs still did not exhibit any drop, while for other 3D PSCs such as FAPbI$_3$, their efficiency may decay to nil after only several days [30]. This further indicates the excellent stability of the PyPbI$_3$ PSCs.
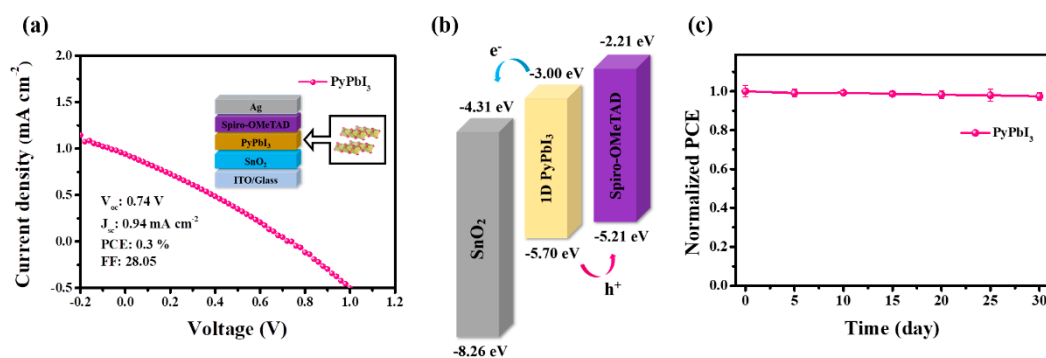
Figure 5. (**a**) J–V curve, (**b**) band energy diagram and (**c**) stability test of PyPbI$_3$ PSC. Inset: PSC devices schematic illustrations.

4. Discussion

In summary, for the first attempt, a 1D perovskitoid, PyPbI$_3$, was employed as an absorbing material in solar cells. The PyPbI$_3$ obtained in this work exhibits a hexagonal crystal structure, instead of the orthorhombic phase reported elsewhere [32], as confirmed by XRD results. More importantly, XPS and FTIR results reveal that there are strong interatomic forces between Py$^+$ cations and inorganic cages, which may help to stabilize its phase. The PyPbI$_3$ exhibited excellent environmental stability compared to 3D FA-based perovskite, as revealed by our stability measurements. Last, PSCs with a lifetime of more than one month employing PyPbI$_3$ as a single absorbing layer was fabricated.

Although the efficiency is not ideal, the kinetically and thermodynamically sTable 1D perovskitoid may play an important role in obtaining long-term stability of PSCs by forming 1D/3D heterojunctions. Moreover, the environmentally sTable 1D perovskitoid, as well as its broadband emission properties [46], have shown great potential in other semiconductor applicationsm including LED, photodetector and memory device. We anticipate that there will be more related 1D perovskitoid work coming in the near future.

Author Contributions: Conceptualization, investigation, methodology, writing—original draft project, F.X.; investigation, methodology, Y.H. and N.L.; supervision, writing—review and editing, Y.L., M.Z. and T.S.; All authors have read and agreed to the published version of the manuscript.

Institutional Review Board Statement: Not applicable.

Informed Consent Statement: Not applicable.

Data Availability Statement: The data presented in this study are openly available in [FigShare] at [10.6084/m9.figshare.14123414 (accessed on 26 February 2021)], reference number [10.1039/c8cc10135c].

Conflicts of Interest: The authors declare no conflict of interest.

References

1. Rong, Y.; Hu, Y.; Mei, A.; Tan, H.; Saidaminov, M.I.; Seok, S.I.; McGehee, M.D.; Sargent, E.H.; Han, H. Challenges for commercializing perovskite solar cells. *Science* **2018**, *361*, eaat8235. [CrossRef] [PubMed]
2. Liu, N.; Wang, L.; Xu, F.; Wu, J.; Song, T.; Chen, Q. Recent Progress in Developing Monolithic Perovskite/Si Tandem Solar Cells. *Front. Chem.* **2020**, *8*, 8. [CrossRef]
3. Kojima, A.; Teshima, K.; Shirai, Y.; Miyasaka, T. Organometal halide perovskites as visible-light sensitizers for photovoltaic cells. *J. Am. Chem. Soc.* **2009**, *131*, 6050–6051. [CrossRef]
4. Xing, G.; Mathews, N.; Sun, S.; Lim, S.S.; Lam, Y.M.; Graẗzel, M.; Mhaisalkar, S.; Sum, T.C. Long-range balanced electronand hole-transport lengths in organic-inorganic CH$_3$NH$_3$PbI$_3$. *Science* **2013**, *342*, 344–347. [CrossRef]
5. Yin, W.-J.; Yang, J.-H.; Kang, J.; Yan, Y.; Wei, S.-H. Halide perovskite materials for solar cells: A theoretical review. *J. Mater. Chem. A* **2014**, *3*, 8926–8942. [CrossRef]

6.   Wang, R.T.; Xu, A.F.; Yang, L.W.; Chen, J.Y.; Kitai, A.; Xu, G. Magnetic-field-induced energy bandgap reduction of per-ovskite KMnF3. *J. Mater. Chem. C* **2020**, *8*, 4164–4168. [CrossRef]

7.   Xu, K.J.; Wang, R.T.; Xu, A.F.; Chen, J.Y.; Xu, G. Hysteresis and Instability Predicted in Moisture Degradation of Perov-skite Solar Cells. *ACS Appl. Mater. Interfaces* **2020**, *12*, 48882–48889. [CrossRef]

8.   Conings, B.; Drijkoningen, J.; Gauquelin, N.; Babayigit, A.; D'Haen, J.; D'Olieslaeger, L.; Ethirajan, A.; Verbeeck, J.; Manca, J.; Mosconi, E.; et al. Intrinsic Thermal Instability of Methylammonium Lead Trihalide Perovskite. *Adv. Energy Mater.* **2015**, *5*, 5. [CrossRef]

9.   Zhou, H.; Chen, Q.; Li, G.; Luo, S.; Song, T.-B.; Duan, H.-S.; Hong, Z.; You, J.; Liu, Y.; Yang, Y. Interface engineering of highly efficient perovskite solar cells. *Science* **2014**, *345*, 542–546. [CrossRef]

10. Bai, Y.; Meng, X.; Yang, S. Interface Engineering for Highly Efficient and Stable Planar p-i-n Perovskite Solar Cells. *Adv. Energy Mater.* **2018**, *8*, 8. [CrossRef]

11. Grancini, G.; Roldán-Carmona, C.; Zimmermann, I.; Mosconi, E.; Lee, X.; Martineau, D.; Narbey, S.; Oswald, F.; De Angelis, F.; Graetzel, M.; et al. One-Year stable perovskite solar cells by 2D/3D interface engineering. *Nat. Commun.* **2017**, *8*, 15684. [CrossRef] [PubMed]

12. Zheng, X.; Wu, C.; Jha, S.K.; Li, Z.; Zhu, K.; Priya, S. Improved Phase Stability of Formamidinium Lead Triiodide Perov-skite by Strain Relaxation. *ACS Energy Lett.* **2016**, *1*, 1014–1020. [CrossRef]

13. Zhu, C.; Niu, X.; Fu, Y.; Li, N.; Hu, C.; Chen, Y.; He, X.; Na, G.; Liu, P.; Zai, H.; et al. Strain engineering in perovskite solar cells and its impacts on carrier dynamics. *Nat. Commun.* **2019**, *10*, 1–11. [CrossRef] [PubMed]

14. Han, Y.; Meyer, S.; Dkhissi, Y.; Weber, K.; Pringle, J.M.; Bach, U.; Spiccia, L.; Cheng, Y.B. Degradation observations of en-capsulated planar CH3NH3PbI3 perovskite solar cells at high temperatures and humidity. *J. Mater. Chem. A* **2015**, *3*, 8139–8147. [CrossRef]

15. Ma, S.; Bai, Y.; Wang, H.; Zai, H.; Wu, J.; Li, L.; Xiang, S.; Liu, N.; Liu, L.; Zhu, C.; et al. 1000 h Operational Lifetime Per-ovskite Solar Cells by Ambient Melting Encapsulation. *Adv. Energy Mater.* **2020**, *10*, 1902472. [CrossRef]

16. Pering, S.R.; Deng, W.; Troughton, J.R.; Kubiak, P.S.; Ghosh, D.; Niemann, R.G.; Brivio, F.; Jeffrey, F.E.; Walker, A.B.; Islam, M.S.; et al. Azetidinium lead iodide for perovskite solar cells. *J. Mater. Chem. A* **2017**, *5*, 20658–20665. [CrossRef]

17. Zheng, C.; Rubel, O. Aziridinium Lead Iodide: A Stable, Low-Band-Gap Hybrid Halide Perovskite for Photovoltaics. *J. Phys. Chem. Lett.* **2018**, *9*, 874–880. [CrossRef] [PubMed]

18. Tombe, S.; Adam, G.; Heilbrunner, H.; Apaydin, D.H.; Ulbricht, C.; Sariciftci, N.S.; Arendse, C.J.; Iwuoha, E.; Scharber, M.C. Optical and electronic properties of mixed halide (X = I, Cl, Br) methylammonium lead perovskite solar cells. *J. Mater. Chem. C* **2017**, *5*, 1714–1723. [CrossRef]

19. Xu, A.F.; Wang, R.T.; Yang, L.W.; Liu, E.E.; Xu, G. An environmentally stable organic–inorganic hybrid perovskite con-taining py cation with low trapstate density. *Crystals* **2020**, *10*, 272. [CrossRef]

20. Wang, Y.; Shi, X.; Wang, G.; Tong, J.; Pan, D. All-inorganic and lead-free BiI3 thin film solar cells by iodization of BiSI thin films. *J. Mater. Chem. C* **2020**, *8*, 14066–14074. [CrossRef]

21. Pandian, M.G.M.; Khadka, D.B.; Shirai, Y.; Umedov, S.; Yanagida, M.; Subashchandran, S.; Grigorieva, A.; Miyano, K. Effect of solvent vapour annealing on bismuth triiodide film for photovoltaic applications and its optoelectronic properties. *J. Mater. Chem. C* **2020**, *8*, 12173–12180. [CrossRef]

22. Hu, W.; He, X.; Fang, Z.; Lian, W.; Shang, Y.; Li, X.; Zhou, W.; Zhang, M.; Chen, T.; Lu, Y.; et al. Bulk heterojunction gifts bismuth-based lead-free perovskite solar cells with record efficiency. *Nano Energy* **2020**, *68*, 104362. [CrossRef]

23. Khadka, D.B.; Shirai, Y.; Yanagida, M.; Miyano, K. Tailoring the film morphology and interface band offset of caesium bismuth iodide-based Pb-free perovskite solar cells. *J. Mater. Chem. C* **2019**, *7*, 8335–8343. [CrossRef]

24. McCall, K.M.; Stoumpos, C.C.; Kontsevoi, O.Y.; Alexander, G.C.B.; Wessels, B.W.; Kanatzidis, M.G. From 0D Cs3Bi2I9 to 2D Cs3Bi2I6Cl3: Dimensional Expansion Induces a Direct Band Gap but Enhances Electron–Phonon Coupling. *Chem. Mater.* **2019**, *31*, 2644–2650. [CrossRef]

25. Umar, F.; Zhang, J.; Jin, Z.; Muhammad, I.; Yang, X.; Deng, H.; Jahangeer, K.; Hu, Q.; Song, H.; Tang, J. Dimensionality Controlling of Cs3Sb2I9 for Efficient All-Inorganic Planar Thin Film Solar Cells by HCl-Assisted Solution Method. *Adv. Opt. Mater.* **2019**, *7*, 7. [CrossRef]

26. Xu, A.F.; Wang, R.T.; Yang, L.W.; Jarvis, V.; Britten, J.F.; Xu, G.; Yang, W. Pyrrolidinium lead iodide from crystallography: A new perovskite with low bandgap and good water resistance. *Chem. Commun.* **2019**, *55*, 3251–3253. [CrossRef]

27. Gao, L.; Spanopoulos, I.; Ke, W.; Huang, S.; Hadar, I.; Chen, L.; Li, X.; Yang, G.; Kanatzidis, M.G. Improved Environmental Stability and Solar Cell Efficiency of (MA,FA)PbI3 Perovskite Using a Wide-Band-Gap 1D Thiazolium Lead Iodide Capping Layer Strategy. *ACS Energy Lett.* **2019**, *4*, 1763–1769. [CrossRef]

28. Li, C.; Song, Z.; Chen, C.; Xiao, C.; Subedi, B.; Harvey, S.P.; Shrestha, N.; Subedi, K.K.; Chen, L.; Liu, D.; et al. Low-bandgap mixed tin–lead iodide perovskites with reduced methylammonium for simultaneous enhancement of so-lar cell efficiency and stability. *Nat. Energy* **2020**, *5*, 768–776. [CrossRef]

29. Xu, A.F.; Wang, R.T.; Yang, L.W.; Liu, N.; Chen, Q.; Lapierre, R.; Isik Goktas, N.; Xu, G. Pyrrolidinium containing perovskites with thermal stability and water resistance for photovoltaics. *J. Mater. Chem. C* **2019**, *7*, 11104–11108. [CrossRef]

30. Xu, A.F.; Liu, N.; Xie, F.; Song, T.; Ma, Y.; Zhang, P.; Bai, Y.; Li, Y.; Chen, Q.; Xu, G. Promoting Thermodynamic and Kinetic Stabilities of FA-based Perovskite by an in Situ Bilayer Structure. *Nano Lett.* **2020**, *20*, 3864–3871. [CrossRef]

31.　Pham, N.D.; Yang, Y.; Hoang, M.T.; Wang, T.; Tiong, V.T.; Wilson, G.J.; Wang, H. 1D Pyrrolidinium Lead Iodide for Efficient and Stable Perovskite Solar Cells. *Energy Technol.* **2020**, *8*, 1900918. [CrossRef]

32.　Miao, Y.; Fan, H.; Wang, P.; Zhang, Y.; Gao, C.; Yang, L.M.; Song, Y.L.; Yang, C.; Liu, C.M.; Jiang, K. From 1D to 3D: Fabrication of CH$_3$NH$_3$PbI$_3$ Perovskite Solar Cell Thin Films from (Pyrrolidinium)PbI3 via Organic Cation Exchange Approach. *Energy Technol.* **2020**, *8*, 2000148. [CrossRef]

33.　Li, N.; Niu, X.; Chen, Q.; Zhou, H. Towards commercialization: The operational stability of perovskite solar cells. *Chem. Soc. Rev.* **2020**, *49*, 8235–8286. [CrossRef] [PubMed]

34.　Burschka, J.; Pellet, N.; Moon, S.-J.; Humphry-Baker, R.; Gao, P.; Nazeeruddin, M.K.; Grätzel, M. Sequential deposition as a route to high-performance perovskite-sensitized solar cells. *Nat. Cell Biol.* **2013**, *499*, 316–319. [CrossRef] [PubMed]

35.　Fan, J.; Ma, Y.; Zhang, C.; Liu, C.; Li, W.; Schropp, R.E.I.; Mai, Y. Thermodynamically Self-Healing 1D–3D Hybrid Perovskite Solar Cells. *Adv. Energy Mater.* **2018**, *8*, 1703421. [CrossRef]

36.　Weber, O.J.; Marshall, K.L.; Dyson, L.M.; Weller, M.T. Structural diversity in hybrid organic-inorganic lead iodide materials. *Acta Crystallogr. Sect. B Struct. Sci. Cryst. Eng. Mater.* **2015**, *71*, 668–678. [CrossRef] [PubMed]

37.　El-Mellouhi, F.; Marzouk, A.; Bentria, E.T.; Rashkeev, S.N.; Kais, S.; Alharbi, F.H. Hydrogen Bonding and Stability of Hybrid Organic-Inorganic Perovskites. *ChemSusChem* **2016**, *9*, 2648–2655. [CrossRef]

38.　Svane, K.L.; Forse, A.C.; Grey, C.P.; Kieslich, G.; Cheetham, A.K.; Walsh, A.; Butler, K.T. How Strong Is the Hydrogen Bond in Hybrid Perovskites? *J. Phys. Chem. Lett.* **2017**, *8*, 6154–6159. [CrossRef]

39.　Liu, N.; Du, Q.; Yin, G.; Liu, P.; Li, L.; Xie, H.; Zhu, C.; Li, Y.; Zhou, H.; Zhang, W.B.; et al. Extremely low trap-state energy level perovskite solar cells passivated using NH2-POSS with improved efficiency and stability. *J. Mater. Chem. A* **2018**, *6*, 6806–6814. [CrossRef]

40.　Wang, R.T.; Xu, A.F.; Chen, J.Y.; Yang, L.W.; Xu, G.; Jarvis, V.; Britten, J.F. Reversing Organic-Inorganic Hybrid Perovskite Degradation in Water via pH and Hydrogen Bonds. *J. Phys. Chem. Lett.* **2019**, *10*, 7245–7250. [CrossRef]

41.　Eperon, G.E.; Paternò, G.M.; Sutton, R.J.; Zampetti, A.; Haghighirad, A.A.; Cacialli, F.; Snaith, H.J. Inorganic caesium lead iodide perovskite solar cells. *J. Mater. Chem. A* **2015**, *3*, 19688–19695. [CrossRef]

42.　Huang, J.; Yuan, Y.; Shao, Y.; Yan, Y. Understanding the physical properties of hybrid perovskites for photovoltaic applications. *Nat. Rev. Mater.* **2017**, *2*, 1–19. [CrossRef]

43.　Xu, W.; He, F.; Zhang, M.; Nie, P.; Zhang, S.; Zhao, C.; Luo, R.; Li, J.; Zhang, X.; Zhao, S.; et al. Minimizing Voltage Loss in Efficient All-Inorganic CsPbI2Br Perovskite Solar Cells through Energy Level Alignment. *ACS Energy Lett.* **2019**, *4*, 2491–2499. [CrossRef]

44.　Matteocci, F.; Cinà, L.; Lamanna, E.; Cacovich, S.; Divitini, G.; Midgley, P.A.; Ducati, C.; Di Carlo, A. Encapsulation for long-term stability enhancement of perovskite solar cells. *Nano Energy* **2016**, *30*, 162–172. [CrossRef]

45.　Yi, H.; Wang, D.; Duan, L.; Haque, F.; Xu, C.; Zhang, Y.; Conibeer, G.; Uddin, A. Solution-processed WO$_3$ and water-free PEDOT:PSS composite for hole transport layer in conventional perovskite solar cell. *Electrochimica Acta* **2019**, *319*, 349–358. [CrossRef]

46.　Wu, G.; Zhou, C.; Ming, W.; Han, D.; Chen, S.; Yang, D.; Besara, T.; Neu, J.; Siegrist, T.; Du, M.-H.; et al. A One-Dimensional Organic Lead Chloride Hybrid with Excitation-Dependent Broadband Emissions. *ACS Energy Lett.* **2018**, *3*, 1443–1449. [CrossRef]